PREDICTION OF HELICOPTER ROTOR AIRLOADS BASED ON PHYSICAL MODELING OF 3-D UNSTEADY AERODYNAMICS

Van Khiem Truong
ONERA
BP 72 - 92322 France

Abstract

The objective of this study is the modeling of 3-D aerodynamic coefficients of a helicopter rotor blade for airload predictions. The approach consists in a careful analysis of the flowfield around a rotor blade. Various 3-D aerodynamic phenomena are shown to be caused by unsteady incoming airflow, advancing and rotating blade motions, the singular behavior of the flowfield at the blade tip and dynamic stall. Modeling of stall is based on the identification of stall onset as a Hopf bifurcation. The 3-D aerodynamic phenomena mentioned above are accounted for by appropriate modifications to the static airfoil characteristics. Correlation studies are conducted with experimental results obtained in a wind tunnel on a rotor with blades having interchangeable rectangular and parabolic/anhedral swept tips. The new aerodynamic model has been implemented in a comprehensive aeroelastic rotor analysis and has permitted the prediction of features of airloads missed by existing models : finite blade effects, particular behavior of dynamic stall.

1. Introduction

Accurate prediction of helicopter rotor loads is a great challenge to rotorcraft engineers. It requires proficiency in modeling rotor dynamics, fuselage dynamics, fuselage aerodynamics, 3-D flow field at the rotor and inflow phenomena. A particular effort is still required for modeling 3-D unsteady aerodynamics that have not been sufficiently explored [1, 2]. New technological developments of helicopters allow flight conditions where the hypothesis of quasi-static aerodynamics is no longer valid. In some research centers, the coupling of aerodynamic CFD solver and structural dynamic codes has been undertaken. However, this methodology which is certainly interesting for understanding 3-D unsteady aerodynamics, demands large CPU time and therefore cannot be used routinely as an engineering tool. This study is concerned with modeling the 3-D unsteady aerodynamic coefficients C_L, C_M and C_D for the prediction of helicopter rotor airloads. Such a methodology must provide predictions of sufficient accuracy to be useful for engineering design.

Due to the importance of 3-D unsteady aerodynamics, it was felt that efforts had to be focused on developing a new model rather than on researching empirical 3-D corrections to the existing "ONERA EDLIN Model" [3, 4]. This model was a big step forward in modeling stall phenomenon. Its strength resides in its analytical formulation in terms of a system of ordinary differential equations, which is appropriate for aeroelastic studies, and in the possibility of determining the constants characterizing the model from independent experiments on oscillating airfoil. However, the implementation of the ONERA EDLIN model in a rotor aeroelastic code has not given entire satisfaction. Particularly, divergence problems occur in calculations involving heavily loaded flight condition and the predicted pitching moment coefficient C_M versus azimuth angle doesn't have the experimentally observed rapid and large variations at stall onset. It is known that such variations lead to large torsional deformation. These two weaknesses of this model are also common to other aerodynamic models. To remedy this situation, preference has been given to the development of a new dynamic stall model based on a Hopf bifurcation. Stall onset has been identified by Tobak et al. [5] to a Hopf bifurcation, i.e. a replacement of a time-invariant equilibrium state of the flow field by a time-varying periodic equlibrium state, as the angle of attack exceeds a critical value. The requirements for the new model are such that it can take into account 3-D aerodynamic phenomena and its parameters are to be determined by carrying out independent experiments. With the notion of a Hopf bifurcation, it has been possible to show the existence of an oscillatory behavior of aerodynamic coefficients with non-negligible amplitudes for an oscillating airfoil [6, 7] and for a rotor blade on the retreating side of the rotor disk [8], in agreement with experimental results. The new model, known as ONERA BH, also predicts rapid and large variations of the C_M coefficient at stall onset. With the 2-D dynamic stall model established and tested with success, efforts are made to extend it to include 3-D effects. A careful analysis of the flow field at the rotor enables to distinguish the following phenomena: radial flow generated by advancing and rotating motions of the blade, 3-D aerodynamic phenomena at the blade tip and near the hub. In the next section it will be shown that the 3-D aerodynamic phenomena mentioned above can be implemented as appropriate modifications of static airfoil section test results.

An evaluation of the capabilities of the new model in predicting rotor airloads was made recently [9]. In this preliminary study, the aerodynamic model was elaborated with only the lift coefficient C_L and the pitching moment coefficient C_M modeled, the values of the drag coefficient C_D were kept quasi-static. This model was implemented in a comprehensive aeroelastic code developed at ONERA [10]. Inflow was described by the Meijer-Drees uniform inflow model. Predictions of rotor loads based on this model were compared with experimental results obtained on a helicopter rotor equipped with rectan-

gular blade tips. Correlation between experimental and calculated results is only fair but is better than that obtained with the old ONERA model. In the present study, the three aerodynamic coefficients are completely modeled. Predictions of rotor loads are compared with experimental results obtained in a wind tunnel on rotors equipped with rectangular and parabolic/anhedral blade tips.

Two test conditions can be distinguished, namely, low load cases with attached flow throughout the rotation cycle and high load cases where the blades are subjected to the stall flow regime on the retreating side of the rotor disk. Even in the attached flow regime, actual rotor analyses which do not use elaborate fluid mechanics equations, such as full-potential flow or Navier-Stokes equations, have difficulties in predicting airloads at the blade tip. It will be shown that the new aerodynamic model is capable of reproducing experimental results in both regimes with a fair agreement and with reasonable CPU time. Use of the METAR prescribed wake model [41] leads to a clear improvement of load predictions over previous ones [9] based on the Meijer-Drees uniform inflow model, especially on the advancing side of the rotor disk.

2.Analysis and modeling of aerodynamic phenomena

2.1. 2-D stall model based on a Hopf bifurcation

The present 3-D aerodynamic model is elaborated through the extension of a recent 2-D stall model, based on a Hopf bifurcation [6, 7]. For the sake of completeness, a brief description of this model is given here.

The 2-D stall model was based on a careful analysis of fluid mechanics mechanisms involved in the dynamic stall process, namely, stall delay and vortex shedding phenomena. The latter is modeled according to the analysis of Tobak et al. [5] who identified stall onset to a Hopf bifurcation. This model has provided the explanation of the non-repeatability of aerodynamic hysteresis loops in stalled flow regimes in terms of flow field initial conditions.

According to the 2-D model, the aerodynamic coefficients $C_a (a = L, M, D)$ are decomposed into :

$$C_a = C_{a_s} + C_{a_i} \tag{1}$$

where C_{a_s} is the "steady" component and C_{a_i} is the "unsteady" component. C_{a_s} is governed by the following ordinary differential equation:

$$\frac{dC_{a_s}}{d\tau} + b\, C_{a_s} = b\, C_{a_s}^{equil}(\alpha(\tau), q(\tau)) + g_1 \frac{d\alpha}{d\tau} + g_2 \frac{d^2\alpha}{d\tau^2} + g_3 \frac{dq}{d\tau} + g_4 \frac{d^2q}{d\tau^2} + \vartheta(\frac{d^3\alpha}{d\tau^3}, \frac{d^3q}{d\tau^3}) \tag{2}$$

where τ is reduced time, $C_{a_s}^{equil}$ is the equilibrium value of the aerodynamic coeffficient which coincides with its static value; b, g_1, g_2, g_3 and g_4 are constants (depending only on Mach and Reynolds numbers, denoted by M and R_e respectively) and $\vartheta(\frac{d^3\alpha}{d\tau^3}, \frac{d^3q}{d\tau^3})$ denotes all the neglected terms of the order $\frac{d^3\alpha}{d\tau^3}, \frac{d^3q}{d\tau^3}$. To study helicopter rotors, it is necessary to consider the whole angle-of-attack domain $[-180°, 180°]$. In the range of $\alpha \in [-40°, +40°]$, the static values are governed by the following relations:

$$\left.\begin{array}{ll} C_{L_s}^{equil} = \frac{\pi}{2\eta_0}(1 + \eta_1\sqrt{f} + \eta_2 f)^2 \sin(\alpha) & + C_{L_0} \\ C_{M_s}^{equil} = (k_0 + k_1 f + k_2 \sin(\pi f^2)) \sin(\alpha) & + C_{M_0} \\ C_{D_s}^{equil} = (c_0 + c_1\sqrt{f} + c_2 f)(1 - \cos(2\alpha)) & + C_{D_0} \end{array}\right\} \tag{3}$$

where $\eta_0, \eta_1, \eta_2, k_0, k_1, k_2, c_0, c_1, c_2, C_{L_0}, C_{M_0}$ and C_{D_0} are constants. For values of $\alpha \in [45°, 180°]$ and $\alpha \in [-180°, -45°]$, simpler relations for aerodynamic coefficients, analogous with those of a flat plate, are used. A linear interpolation is made for values belonging to $]-45°, -40°[$ and $]40°, 45°[$. When the airfoil is maintained stationary, the separation point f is defined as:

$$f = \begin{cases} 1 - 0.3\exp[(\alpha - \alpha_1)/s_1] & : \alpha \le \alpha_1 \\ 0.04 + 0.66\exp[-(\alpha - \alpha_1)/s_2] & : \alpha > \alpha_1 \end{cases} \tag{4}$$

where s_1 and s_2 are constants and the value of α_1 is very near to α_{cr}, the critical value of angle of attack for static stall onset. When the airfoil is undergoing an oscillatory motion in pitch, f is replaced by f' defined as:

$$\frac{df'}{d\tau} + \frac{1}{T_f} f' = \frac{1}{T_f} f \tag{5}$$

where T_f is a constant. Equations (3), (4) and (5) originate from the Leishman-Beddoes model [11], with a novel formulation for $C_{D_s}^{equil}$.

For the unsteady behavior of aerodynamic coefficients, one distinguishes two regimes according to the temporal history of the angle of attack α: a periodic time-varying equilibrium state which is established when α, increasing from a small value, attains a critical value α_{cr} and a decay regime of the above periodic time-varying state when α decreases from high to low values. It is shown [6] that the lift coefficient C_L is governed by a Van-der-Pol-Duffing type equation during the first of these regimes:

$$\frac{d^2C_{z_i}}{d\tau^2} - \omega_S(\beta_L^+ - \gamma_L^+ C_{z_i}^2)\frac{dC_{z_i}}{d\tau} + \omega_S^2(C_{z_i} - \eta_L^+ C_{z_i}^3 - a_{2,L}^+ C_{z_i}^2) = -E_L^+\omega_S\frac{d\alpha}{d\tau} - D_L^+\omega_S\frac{d^2\alpha}{d\tau^2} \tag{6}$$

where the constants with a supercript + characterize the growth regime. The simplest way of modeling the decay regime is by a damped oscillator:

$$\frac{d^2C_{z_i}}{d\tau^2} - \omega_S\beta_L^-\frac{dC_{z_i}}{d\tau} + \omega_S^2 C_{z_i} = 0 \tag{7}$$

where β_L^- is negative. In total, equations (6) and (7) require 8 parameters. The pitching moment coefficient C_M and the drag coefficient C_D are governed

respectively by equations analogous to (6) and (7).

The parameter values of the model are determined from experiments on airfoils maintained stationary and undergoing oscillatory motion in pitch. In the present model, plunging motion is neglected. Static airfoil test section results of aerodynamic coefficients are modeled for values of Mach numbers in the range [0.1, 1.]. There are also corrections to account for the value of the Reynolds number. As the studied airfoil is usually not symmetrical, one needs to model aerodynamic coefficients differently according to $\alpha \leq 0$ or $\alpha \geq 0$. Figure 1 shows static OA 209 airfoil test section results of aerodynamic coefficients in the range $\alpha \in [0°, +40°]$ and modeling results: there is a good correlation. The values of parameters in equation (2) are determined from experiments on oscillating airfoils in the attached flow regime. The values of parameters in equations (6) and (7) are resolved from experiments on oscillating airfoils in the stalled flow regime.

In the ONERA EDLIN model, aerodynamic coefficients are also decomposed into two components governed by the same type of ordinary differential equations but these have different physical meanings. According to this old model, the first component of the lift coefficient is governed by an equation practically identical to equation (2) but with a different physical interpretation for the first term on the right hand side of the equation: the static values of aerodynamic coefficients appear explicitly in equation (2) while in the old model this term represents the linear value. The advantage of this modification will appear in the next section for the incorporation of 3-D aerodynamic effects. The second component is governed in the old model by an ordinary differential equation corresponding to a damped oscillator.

Figure 2 presents an example of predictions for the NACA 0012 airfoil in attached and stalled flow regimes. This example reveals the following characteristics:

(i) an oscillatory behavior of the aerodynamic coefficients: this is predicted by Geissler et al. [12], based on a CFD simulation (see alo discussions in [7]) and it cannot be neglected as long as the oscillatory amplitude is not negligible ;

(ii) large and rapid variations of $C_M(\alpha)$ and $C_D(\alpha)$ at stall onset due to their respective unsteady components : $C_L(\alpha)$ also has such variations but they are less visible. The ONERA EDLIN model predicts a smoother behavior for unsteady components ;

(iii) the mean values of the unsteady components of the aerodynamic coefficients averaged over a hysteresis loop are not equal to zero and are positive. In the ONERA EDLIN model, the mean value is nearly equal to zero.

The above findings show that the proposed model has good features for predicting rotor airloads :

(i) From experiments on rotors [8, 13], there is evidence of the existence of oscillatory behavior of airloads associated with the stall phenomenon. This is particularly true in heavily loaded configurations where the amplitude of oscillations in sectional lift and pitching moment coefficients attain nearly half their maximum amplitude ;

(ii) It is commonly known that a large and sudden change in pitching moment due to stall leads to large fluctuations in rotor blade torsional loads : a numerical simulation by Yen and Yuce [14] demonstrates that a nose-down impulse pitching moment resulting from retreating blade stall is sufficient to reproduce stall-flutter characteristics ;

(iii) The third finding means that there is a continuous increase of mean values of C_L and C_D coefficients averaged over a rotation cycle as flight conditions enter into deeper stall. This leads to a continuous increase of rotor lift and power with rotor loading in deep stall. The ONERA EDLIN model, or any other model which cannot provide this feature, is unable to converge to a set of trim conditions in a very deep stalled flow regime.

2.2. Analysis of 3-D aerodynamic phenomena

Various 3-D aerodynamic phenomena in the flow field around a rotor blade (cf. figure 3) can be identified :

(i) unsteady incoming flow velocity due to the rotating motion of the blade ;

(ii) radial flow along the blade span generated by rotating and advancing motions of the blade ;

(iii) 3-D aerodynamic phenomena at the blade tip ;

(iv) other 3-D aerodynamic phenomena.

2.2.1. Unsteady incoming flow velocity

This effect can be studied in 2-D by considering an oscillating airfoil immersed in a periodic time-varying stream. Several authors have studied this unsteady phenomenon by using experimental or theoretical approaches, but it has been noted recently [15, 16] that no entirely satisfactory correlation studies between experiments and models have been made. The present modeling makes use of unsteady corrections proposed by Peters [17].

2.2.2. Radial flow

The effect of radial flow was first mentionned by Himmerskamp [18]. This author observed a large increase in lift coefficient C_L on a rotating airscrew at span sections near the hub, practically a doubling of its 2-D value. He attributed this increase to a stall delay phenomenon generated by radial flow. Extensive experimental and numerical investigations were then directed towards the study of radial flow. It was not detected experimentally for non separated rotating boundary layers [19]. Due to computational ressources available at the time, numerical simula-

tion were limited to the analysis of laminar boundary layers. Harris [20] made a remarkable synthesis of the experimental and theoretical publications prior to 1966. This author concluded that the flow field around an advancing rotor blade is similar to the one around a swept airfoil. He noted that rotation effects are similar to sweep effects. Harris' modeling, which includes sweep effects and unsteady aerodynamics, was sufficient to reproduce helicopter rotor loads measured in the 70's.

The modeling of the advancing blade motion by Harris consists essentially in replacing static section test results on a rectangular airfoil by those on a swept airfoil. The value of the sweep angle seen by a rotating blade would not necessarily coincide with its instantaneous value: there is a possiblity of unsteady sweep effects. Harris postulated a quasi-static approximation. Leiss [21] has proposed a model of unsteady sweep effects but, as noted by Leishman [22], this has not been validated against experiments.

There are very few experiments on swept airfoils or wings. From a search through the literature, 4 experimental studies were found :

- static measurements by Purser and Spearman [23] on wings with sweep angles varying between 0^o and 70^o ;
- static and dynamic measurements, carried out at ONERA and reported by Costes [24], on a wing with sweep angles to $-20^o, 0^o$ and $+20^o$;
- static and dynamic measurements by St.Hilaire et al. [25, 26] on airfoils with sweep angles equal to 0^o and 30^o ;
- static and dynamic measurements by Lorber et al. [27] on a wing with sweep angles of $0^o, 15^o$ and 30^o .

Sweep effects are observed in both the static and the dynamic behavior of aerodynamic coefficients. Usually it is assumed that the flow velocity field in a chordwise section normal to the leading edge of a swept wing has the same behavior as the one taken in the same conditions on a rectangular wing. This assumption probably holds for sufficiently small angles of attack α. There is agreement between experiments on an increasing delay of stall onset as the sweep angle Λ increases. After stall onset, the flow behavior around a swept airfoil differs from that on an unswept airfoil. Consequently, the shape of 2-D aerodynamic characteristics changes with Λ. Experiments show that the hysteresis loops of aerodynamic coefficients in the stalled flow regime become narrower as Λ increases.

The set of measurements by Purser and Spearman are very interesting because they cover a large range of sweep angles. Unfortunately the accuracy of the drag coefficient measurements is poor. The whole set of experimental results of Lorber et al. was not available, so that an analysis was carried out on the limited set of published results. Experimental measurements of the lift coefficient C_L by Purser and Spearman have been analyzed by Leishman [22], on the basis of the Leishman-Beddoes model. His results are used here to deduce sweep effects on lift-curve characteristics, namely dependence on Λ of the critical value of the stall onset angle of attack α_{cr} and of the parameters s_1 and s_2 (cf. equation (4)). Due to the lack of available experimental data, sweep effects for sectional characteristics of moment and drag coefficients are accounted for only through the variation of $\alpha_{cr}(\Lambda)$ which is established for C_L. The parameters characterizing the unsteady component of aerodynamic coefficients are kept constant with Λ, except for the value of T_f (cf. equation (5)). An empirical relationship of T_f decreasing with Λ is used, in order to get a narrowing of hysteresis loops as Λ increases.

The issue of rotation effects has been raised recently in conjunction with the performances of tilt rotor and of horizontal axis wind turbines. In the former case, experiments show clearly an increase in lift coefficient values for blade sections near the hub. Narramore et al. [28] succeed in reproducing the increase of C_L by using a 3-D Navier-Stokes code. These authors interpret this increase as being due to the stall delay associated with rotation. Their numerical simulations are consistent with those of Banks and Gadd [29] who predicted no separation near the hub of a rotating blade, based on laminar boundary layer equations. In the case of wind turbines, measurements made by Ronsten [30] show evidence of the stall delay phenomenon for inboard blade sections. Snel et al. [31], using a quasi 3-D approximation of boundary layer equations, reproduce qualitatively the stall delay effect on a wind turbine. They give a physical explanation of the phenomenon: rotation effects become large for separated flow. Corrigan et Schillings [32] suggest modeling rotation effects through an increased value of the stall angle of attack, α_{cr}, deduced from numerical results of Banks and Gadd. Practically this leads to a doubling of α_{cr} at the 20% R (R: blade radius) inboard section and no separation at the hub. Vansteenberghe et al. [33] have also suggested an empirical model of rotation effects based on the numerical results of Snel at al. [31]. Their procedure consists in increasing the level of the static curves of the aerodynamic coefficients when the angle of attack is beyond its critical value α_{cr} which is kept unchanged. It appears that the correct approach is to increase α_{cr} and to modify also the shape of the 2-D aerodynamic characteristics: such a procedure is analogous to the one used for incorporating sweep effects.

The experimental results of the FFA [30] concerning lift coefficients at sections $75\%R, 55\%R$ and $30\%R$, for nonrotating conditions, are shown in figure 4. Under rotating conditions, the angle of attack is corrected by Snel et al. [31] for induced velocity effects and their results are also depicted in figure

4. The present model is capable of reproducing the experimental results (cf. equation (4)), the values of parameters varying according the span section location considered. Concerning C_M and C_D coefficients, there are no experimental values available. The numerical simulation of Snel et al. surprisingly shows that the values of C_M are affected by rotating blade motion even in the attached flow regime, giving a more nose-down value for the sections nearer the hub. This behavior needs further investigation.

The corrections to α_{cr}, s_1 and s_2 due to sweep and rotation effects are additive. These effects have beneficial consequences for rotor lift and power. To evaluate the reality of rotation effects on helicopter rotor blades, a thorough examination of hover experimental results is suggested.

2.2.3. Aerodynamic phenomena at the blade tip

Maier and Bousman [34] have recently emphasized the predominance of the action of sectional aerodynamic pitching moments C_M at the outer 10% of the blade in creating the large oscillating pitch-link loads for flight in the attached flow regime. These authors have noticed a peculiar behavior of C_M at the blade tip: a positive C_M coefficient in the first quadrant of the rotor disk with a rapid reversal of sign in the second quadrant. After having examined various possible causes for this behavior, they have attributed it to a 3-D unsteady phenomenona. Costes [39] modified the ONERA EDLIN model to take into account the behavior of the pitching moment coefficient at the blade tip. He concluded that unsteady transonic effects were responsible. In a recent publication [9], the physical phenomenon responsible is associated to "finite swept wing effects". The description of the phenomenon which is still not clear is again addressed below.

Let us first consider the experimental facts about the behavior of the aerodynamic pitching moment C_M of swept wings. Measurements show that at blade sections near the wing tip, C_M has a particular behavior different from 2-D. Values measured at sections near the tip are depicted in figure 5. The data are taken from experiments done at ONERA on a swept wing with $\Lambda = -20^o, 0^o, 20^o$ and at UTRC on a swept wing with $\Lambda = 0^o, 15^o, 30^o$. In the range of $\Lambda > 0$, these two experiments are in qualitative agreement, although they are conducted on wings with different airfoils section, namely OA 209 and SSC-A09 airfoils respectively. As shown in figure 5, the pitching moment acquires a positive component near the wing tip. Then, as α increases, it goes through to negative values which may be large, if Λ is negative. The UTRC measurements at $\Lambda = 0$ show a slight decrease of C_M values as α increases. Experiments made by Szafruga and Ramaprian [35] on a rectangular wing show that C_M decreases to the level of its 2-D value for sufficiently high values of α. For the sake of continuity, it is assumed that the C_M value at the wing tip for $\Lambda < 0$ will attain its 2-D value at high values of α. It is possible to decompose C_M into:

$$C_{M_s}(r_S, \Lambda) = C_{M_{s0}} + C_{M_{s1}}(r_S, \Lambda) + C_{M_{s2}}(r_S, \Lambda) \quad (8)$$

where $C_{M_{s0}}$ denotes the 2-D value, $C_{M_{s1}}$ the positive component, $C_{M_{s2}}$ the negative component of C_M and r_S is the blade section location. The component $C_{M_{s2}}$ is practically absent for $\Lambda = 20^o$ (swept back wing) and rises as Λ decreases from the zero value. The value of the angle of attack for the onset of the $C_{M_{s2}}$ value shifts from several degrees for $\Lambda = 0^o$ to a few degrees for $\Lambda = -20^o$. Furthermore, it decays to zero beyond $0.3c$ (c : chord length) from the wing tip. In agreement with Lorber et al. [27] $C_{M_{s2}}$ is associated to the action of the tip vortex. The positive component $C_{M_{s1}}$ has a different spatial dependence with a characteristic length larger than for $C_{M_{s2}}$. In the preliminary study [9] this was erroneously attributed to the influence of the tip vortex; indeed, $C_{M_{s1}}$ is present before the formation of the tip vortex. The present assumption concerning the physical origin of $C_{M_{s1}}$ is supported by the recent work of Beddoes [36]. This author has presented a method for treating separation on a blade with complex tip planform by extending the Kucheman idealization. According to Kucheman, the behavior of the sectional lift coefficient C_L and the aerodynamic centre location x_{ac} change near the wing tip, and these "finite wing effects" depend on the sweep angle Λ of the blade. For a sweptback wing, x_{ac} (which usually has a value greater than 0.25) decreases from its 2-D value near the tip. As the indicial pitching moment response (cf. for instance [37]) contains an indicial circulatory response multiplied by the factor $(0.25 - x_{ac})$, the C_M at sections near the tip increases from its 2-D negative values and may become positive.

The negative component $C_{M_{s2}}$, associated with the tip vortex, cannot be accounted for by lifting line theory or by full-potential equations but only by Navier-Stokes equations. Wake and Lorber [38] using a 3-D Navier-Stokes code predicted the lift coefficient, but failed to obtain the pitching moment coefficient at the wing tip. There are still improvements to be made in CFD simulations in order to provide predictions for the drag coefficient which is more difficult to evaluate than C_M. Determination of the drag coefficient is essential for prediction of rotor power.

Finite swept wing effects are observed in the behavior of C_M, C_D and C_L. In this study, the three aerodynamic coefficients are modeled on the basis of the scarce experimental results on swept wings, covering sweep angles from -20^o to 30^o. For conventional helicopter flight, the range of sweep angles is $[-40^o, 40^o]$. Therefore, experiments on swept wings with a larger range of sweep angles are badly needed. It is also possible for the model to incorporate CFD

results if they are available. In the present case, the modeling of finite swept wing effects, although extrapolated from the experimental data, will be tested against experimental rotor loads in order to evaluate its validity.

2.2.4. Other 3-D aerodynamic phenomena

It is assumed that interference between the main rotor and other parts of the helicopter such as the tail rotor, the fuselage and the hub are negligible. Recent experimental work, based on laser velocimetry studies [40], shows that the effect of the aerodynamic forces produced in the hub region on the rotor blade may be large. Particularly, high turbulent intensity values are seen on the retreating side of the rotor, at mid-span of the blade. In these conditions, stall onset may occur at lower angle of attack than usual. This merits further investigation.

3. Correlation studies

3.1. General considerations

The present aerodynamic model has been implemented in a comprehensive aeroelastic rotor analysis elaborated at ONERA [10] with a modular design : an aerodynamic module for the computation of aerodynamic coefficients and reduced velocity, a structural module for the computation of blade deflections and a mathematical module for the resolution of aeroelastic equations governing the motion and the deflections of the rotor blades. The original module for aerodynamic coefficients, based on the ONERA EDLIN model, is here replaced by a new module describing the present ONERA BH model. The inflow model can be either the Meijer-Drees uniform inflow or the METAR prescribed wake model [41, 42]. The mathematical solver module is based on a harmonic response solution method, i.e. the aerodynamic response of the blade is assumed to be periodic with a frequency equal to the rotation frequency of the blade. In a preliminary study based on the new model [9], inflow is described by the Meijer-Drees model. It is well known that a uniform inflow does not provide good predictions of airloads on the advancing side of the rotor disk. The rotor analysis with the new aerodynamic module was therefore coupled to the METAR model following a method proposed by Lyoen [43] where blade circulations are considered as unknowns for the resolution of the aeroelastic equations, This ensures numerical convergence.

In the next section, calculations with the model are correlated with experiments conducted in a wind tunnel on a helicopter rotor equipped with interchangeable rectangular and parabolic/anhedral blade tips [44, 45]. From the hub to the tip the blade has OA 213 and OA 209 airfoil sections with a transition zone. Airloads are measured with pressure transducers mounted in five blade sections at the following spanwise positions : $r/R = 0.975, 0.915, 0.825, 0.70$ and 0.50, where R denotes the rotor radius. Blade deflections are obtained from the response of 30 strain gauges placed on a specially instrumented blade using the SPA strain pattern analysis technique [46]. Experiments are focused on moderate and high speed forward flights (advance ratio $\mu = 0.3 - 0.55$). Loads obtained are consistent with those reported in the literature.

The present modeling considers the blade as consisting of only OA 209 airfoil sections, some empirical corrections are used to account for the OA 213 airfoil sections. The wind tunnel results are analyzed for tests in both attached and stalled flow conditions.

3.2. Tests in attached flow conditions

3.2.1. Rectangular blade tips

Figures 6 and 7 show measured and predicted sectional normal force versus azimuth angles for two test conditions on the rotor with straight tips : a/ $(C_L/\sigma = 0.08, \mu = 0.30)$, b/$(C_L/\sigma = 0.08, \mu = 0.40)$. Predicted values are based on the ONERA EDLIN model with the METAR inflow model, the ONERA BH model with the Meijer-Drees and the METAR inflow models respectively. Predictions from the new model with the METAR inflow is fair : inaccuracy occurs primarily in the azimutal range $[60^o, 120^o]$ for all span sections. However, comparison between the two ONERA models reveals features captured by the new model. At blade span locations near the tip ($97\%R$ and $91\%R$), two humps are clearly shown by the new model at azimuth angles near 60^o and 300^o, while in the old model only the first one is slightly visible. As these humps don't occur in the prediction with the Meijer-Drees inflow, they are associated with blade-vortex interaction. This is in agreement with the conclusion of Hooper [47] who draws the common features of airloads among various rotors. In his seminal work, Hooper points out that high harmonic loading is dominated by blade-vortex interaction near the blade tip on the advancing side for flight in attached flow condition. The blade experiences interaction with the wakes produced by previous blades, leading to an up-down impulse in airloads near $\psi = 60^o$ and a down-up impulse near $\psi = 300^o$. As μ increases to 0.4 (cf. figure 7), the down-up impulse is less visible. There is however an undulatory behavior for $C_N M^2$ for span locations near the tip and in the azimutal range $[90^o, 210^o]$. For higher advance ratios (not shown), this undulatory behavior disappears. This is presumably a peculiar feature due to the coupling of the rotor analysis with the METAR model.

In figure 8, experimental and predicted values of sectional normal pitching moment are shown for the case $\mu = 0.40$. Prediction is improved by the new

aerodynamic model at every blade span location. Maier and Bousman [34] point out that, for span locations near the blade tip, sectional pitching moments have a nose-up behavior in the first quadrant followed by a rapid reversal of sign at the end of the first quadrant. The present model succeeds in reproducing this behavior by accounting for finite swept wing effects. To give an understanding of these effects, it is necessary to consider the values of the sweep angle, Mach number and angle of attack at the $97\%R$ section (cf. figure 9). In the azimuthal range $[0^o, 50^o[$, the sweep angle and the angle of attack α are positive ; therefore, the pitching moment is positive. At ψ near 50^o, as Mach number reaches nearly 0.90 and α is still positive, C_M rapidly decreases to negative values. Subsequently, α becomes negative over a small azimuthal range, C_M rises from negative values to less negative values (eventually attaining positive values for flights with higher thrust levels) and returns to its initial level when α becomes positive : it has an impulsive behavior. The experimental results show that $C_M M^2$ in the third quadrant has negative values for the section at $97\%R$, while it has positive values for the section at $91\%R$. This behavior illustrates well the influence of the tip vortex. Indeed, in this azimuthal range, α attains high positive values and Λ is negative ; therefore, the C_M coefficient near the tip becomes negative due to the presence of the tip vortex. For the span location at $50\%R$, C_M has a higher negative values than those provided by 2-D section test results. These high values are obtained by empirically accounting for rotation effects. However, this decrease in C_M is rather large, so it should probably not be entirely attributed to rotation effects. This question merits further investigation.

One may ask why the new model succeeds in capturing features related to the blade-vortex interaction which are missed by the old model. A calculation made with the ONERA EDLIN model and imposing the measured torsional bending shows the hump at ψ near 60^o which is not visible with the calculated torsional bending. Since torsional bending behavior is governed by pitching moment, the good prediction of C_M by the new model is presumably the origin of the improvement in the predicted values of C_N.

The quality of the correlation between experimental and predicted airloads has still to be improved with regard to amplitude and phase at $\psi = 90^o$. According to [48, 49] it seems that inflow modeling using a free wake instead of a prescribed wake leads to more negative lift at ψ near 90^o, which would improve correlation. The phase shift remains the most important discrepancy to resolve. It is quite large, of the order of 30^o, and is observed in the predictions of almost every aeroelastic code. The phase shift is transmitted to predicted values of the blade tip torsional deflection Φ, as shown in figure 10. Despite this, the predictions of Φ are an improvement over the old model, both in amplitude and high harmonic content, due to a better prediction of C_M. The sources of excitation of the blade tip torsional deflection are the large variations of C_M near $\psi = 60^o$ and for flights with high thrust levels the impulse caused by values of $\alpha < 0$.

3.2.2. Sweptback parabolic/anhedral blade tips

The aerodynamic model developed for the rotor equipped with rectangular blade tips is also used for the rotor with parabolic/anhedral blade tips by modifying the geometric sweep angle at the blade tip. The present version of the rotor analysis provides only calculations for sections normal to the local leading edge of the blade. Figure 11 shows experimental and predicted values of sectional normal force versus azimuth angles for the test case with $C_L/\sigma = 0.08$ and $\mu = 0.40$. The conditions of this test are the same as those of the test on the straight tipped rotor blades. Except for the blade span location at $97\%R$, where there is geometric incompatibility between the rotor analysis and the experimental results, correlation is fair and the level of accuracy is the same as for the previous rotor. The hump produced by blade-vortex interaction at $\psi = 60^o$ on the sectional normal force is still visible but is attenuated due to the planform of the blade tip. Calculations using a full-potential code for the aerodynamics [45] are also shown in figure 11. The quality of correlation obtained with the present aerodynamic model is of the same order as that of the full potential analysis but with less CPU time. Figure 12 shows experimental and predicted values of the sectional pitching moment : the same conclusions as above can be drawn except that the large decrease of $C_M M^2$ at span location $69\%R$ is not well reproduced by the model. The blade tip deflection is shown in figure 13. Calculated values compared to experimental results consistently show a forward phase shift, as for the straight blade tips.

3.3. Tests in stalled flow conditions

According to the new model, stall vortices induce an oscillatory behavior of aerodynamic coefficients with a frequency equal to the Strouhal frequency which is not a multiple integer of the blade rotation frequency. It is therefore mandatory to use a time marching procedure for solving the aeroelastic equations governing the blade. However in its present version the aeroelastic code is implemented only with a numerical solver which assumes a periodic aerodynamic response. In order to get an evaluation of the new model, calculations are carried out assuming no vortex-induced oscillations, i.e. no unsteady component of the aerodynamic coefficients. When numerical convergence is obtained, airloads are recalculated with the values obtained for blade deflections.

Only a test case on the swept tipped rotor is pre-

sented. Figure 14 shows experimental and predicted values of the normalized normal force $C_N M^2$ for the conditions $C_L/\sigma = 0.11$ and $\mu = 0.40$. Correlation is fair with only a small phase shift between experimental and calculated results. In the azimutal range $[240°, 360°]$, corresponding to the establishment of the stalled flow regime, one notices an oscillatory behavior of the airloads. Effects are not important for the sectional normal force but cannot be ignored for the sectional pitching moment (cf. figure 15). Particularly, the rise of $C_M M^2$ is practically instantaneous and it provides a strong source of excitation for blade deflections. Yen and Yuce [14] have pointed out that a nose-down impulse behavior of $C_M M^2$ on the retreating side of the rotor disk is mandatory for reproducing stall flutter characteristics. The dominant physical mechanism for excitation of the blade tip deflection in this test case is dynamic stall, prevailing over the mechanisms present in attached flow condition.

Correlation for $C_M M^2$ deteriorates for inboard span locations at $69\%R$ and $50\%R$. Rotation effects have been suggested in order to remedy deficiencies in predictions at these section locations. In this test configuration, such effects cannot explain the large values of $C_M M^2$ at around $\psi = 230°$ at the $50\%R$ span location. Note that these values correspond in fact to quite large values of C_M that are attenuated by the factor "M^2". They are undeniably caused by the stall phenomenon. The hub motion (cf. § 2.2.4) may cause a decrease in the critical onset angle of attack at the blade mid-span. In order to get a better understanding, airload measurements at inboard locations less than $50\%R$ are needed.

The prediction of rotor power by the new model for the swept tipped rotor in stalled flow conditions with advance ratio $\mu = 0.40$ is improved over the old model (cf. figure 16). There is still a discrepancy between experimental and model results which may be resolved by a time marching solving procedure.

4. Conclusions

A model for 3-D aerodynamic coefficients of helicopter blades has been developed on the basis of a careful analysis of the flow field around the main rotor blade. The model has been introduced into a comprehensive aeroelastic rotor analysis and predictions of airloads were made for rotors tested in a wind tunnel. Both rectangular and parabolic/anhedral blade tips were considered. The model accounts for finite swept wing effects which improve the prediction of the pitching moment. This in turn improves other predictions including sectional normal forces and blade tip deflections. The quality of the correlation between predictions and experimental results is only fair but is of the same order as when using an analysis based on full potential equations. In the particular case of stalled flow on the retreating blade, the aeroelastic analysis used does not permit a complete evaluation of the model, however two important features missed by other models are captured, namely :

(i) a rapid and large variation of sectional pitching moment at stall onset This is a necessary condition for reproducing stall-flutter characteristics.

(ii) an increased mean value of the unsteady aerodynamic coefficients averaged over a rotation cycle. Hence, the prediction of a continuous increase of lift and rotor power can be expected when entering deep stall.

Predictive calculations suggest that swept tip planforms can be correctly accounted for by the model. Confirmation of this requires further comparisons with test results on rotor blades with different planforms.

Acknowlegments

This study was partially funded by DRET. The author would like to thank Mr. D. Petot for having introduced him to the aeroelastic rotor analysis and for having provided him with the loads predictions using the ONERA EDLIN model and Mr. P. Beaumier for having provided him the full potential results.

References

[1] McCroskey W.J., *Special Opportunities in Helicopter Aerodynamics*, NASA TM 84396, 1983.

[2] Philippe J.J. and Roesch P., Dequin A.M., Cler A., *Recent advances in helicopter aerodynamics*, AHS-NAI Seminar on "The theoretical Basis of Helicopter Technology", Nanjing, China, November 1985.

[3] Dat R., Tran C.T. and Petot D., *Modèle phénoménologique de décrochage dynamique sur profil de pale d'hélicoptère*, XVIe Colloque d'Aérodynamique Appliquée (AAAF), Lille (France), November 1979.

[4] Petot D., *Modélisation du Décrochage Dynamique par Equations Différentielles* , La Recherche Aérospatiale, vol. 5, pp.59-72, 1989.

[5] Tobak M. and Chapman G.T., *Nonlinear Problems in Flight Dynamics Involving Aerodynamic Bifurcations*, AGARD Symposium on Unsteady Aerodynamics - Fundamentals and Applications to Aircraft Dynamics. Germany, paper No. 25, May 1985.

[6] Truong V.K., *Modèle de décrochage 2-D basé sur la notion de bifurcation de Hopf*, La Recherche Aérospatiale, No. 4, pp. 55-65, 1993.

[7] Truong V.K., *A 2-D Dynamic Stall Model Based on a Hopf Bifurcation*, Nineteenth European Rotorcraft Forum, Cernobbio (Como) Italie, paper No. C23, September 1993.

[8] Truong V.K. and Costes J.J., *Oscillatory Behavior of Helicopter Rotor Airloads in the Blade Stall Regime*, AIAA Journal of Aircraft vol. 32, No. 5, pp.1148-1149, 1995.

[9] Truong V.K., *Prévisions des charges sur une pale d'hélicoptère basées sur le modèle de bifurcation de Hopf*, XXXIe Colloque d'Aérodynamique Appliquée (AAAF), Paris (France), 27-29 mars 1995.

[10] Bessone J. and Petot D., *Calculs du comportement aéroélastique des rotors comparés à l'expérience*, La Recherche Aérospatiale, vol. 1, pp.3-14, 1995.

[11] Leishman J.G. and Beddoes T.S., *A Semi-Empirical Model for Dynamic Stall*, J. American Helicopter Society vol. 34, pp. 3-17, 1989.

[12] Geissler W. and Vollmers H., *Unsteady Separated Flows on Rotor - Airfoils*, Eighteenth European Rotorcraft Forum, Avignon, France, paper No. 79, September 1992.

[13] Coleman C.P. and Bousman W.G., *Aerodynamic Limitations of the UH-60A Rotor*, American Helicopter Society Aeromechanics Specialists Conference, California (U.S.A.), January 1994.

[14] Yen J.G. and Yuce M., *Correlation of Pitch-Link Loads in Deep Stall on Bearingless Rotors*, J. American Helicopter Society, vol. 37, pp. 4-15, 1992.

[15] Favier D., Belleudy J. and Maresca C., *Influence of Coupling Incidence and Velocity Variations on the Airfoil Dynamic Stall*, AHS 48th Annual Forum, Washington D.C., June 3-5 1992.

[16] Van der Wall B.G. and Leishman J.G., *The Influence of Variable Flow Velocity on Unsteady Airfoil Behavior*, Eighteenth European Rotorcraft Forum, paper No. 81, Avignon, France, September 1992.

[17] Peters D.A., *Toward a Unified Lift Model for Use in Rotor Blade Stability Analyses*, J. American Helicopter Society vol. 30(3), pp. 32-42, 1985.

[18] Himmelskamp H., *Profile investigations on a rotating airscrew*, Doctoral Thesis, Göttingen, 1945.

[19] McCroskey W.J., *Measurements of Boundary Layer Transition, Separation and Streamline Direction on, Rotating Blades*, NASA TN D-6321, 1971.

[20] Harris F.D., *Preliminary Study of Radial Flow Effects on Rotor Blades*, J. American Helicopter Society, vol. 11, pp. 1-21, 1966.

[21] Leiss U., *Unsteady Sweep - A Key to Simulation of Three - Dimensional Rotor Blade Airloads*, Vertica, vol. 10, pp. 341-351, 1986.

[22] Leishman J.G., *Modeling Sweep Effects on Dynamic Stall*, J. American Helicopter Society, pp. 18-29, 1989.

[23] Purser P.E. and Spearman M.L., *Wind-Tunnel Tests at Low Speed of Swept and Yawed Wings Having Various Plan Forms*, NACA TN 2445, 1951.

[24] Costes J.J. and Petot D., *Forces aérodynamiques couplées dues au décrochage instationnaire sur une aile de grand allongement oscillant à grande amplitude*, AGARD/SMP Sorrento,Italy, 1990.

[25] St. Hilaire A.O., Carta F.O., Fink M.R. and Jepson W.D., *The Influence of Wing Sweep on the Aerodynamic Loading of an Oscillating NACA 0012, Airfoil. Volume I - Technical Report*, NASA CR-3092, 1979.

[26]St. Hilaire A.O. and Carta F.O., *The Influence of Sweep on the Aerodynamic Loading of an Oscillating NACA 0012 Airfoil. Volume II - Data Report*, NASA CR-145350, 1979.

[27] Lorber P.F., Carta F.O. and Covino A.F., *An Oscillating Three-Dimensional Wing Experiment: Compressibility, Sweep, Rate, Waveform, and Geometry Effects on Unsteady separation and Dynamic stall*, UTRC Report R92 - 958325-6, 1992.

[28] Narramore J.C. and Vermeland R., *Navier-Stokes Calculations of Inboard Stall Delay Due to Rotation*, AIAA J. Aircraft, vol. 29 (1), 1992.

[29] Banks W. and Gadd G., *Delaying Effect of Rotation on Laminar Separation*, AIAA Journal, vol. 1, No. 4, pp. 941-942, 1963.

[30] Ronsten G., *Static Pressure Measurements on a rotating and a non-rotating wind turbine blade. Comparison with 2D calculations*, J. Wind Engineering and Industrial Aerodynamics, vol. 30, pp.105-118, 1992.

[31] Snel H., Houwink R. and Bosschers J., *Sectional Prediction of Lift Coefficients on rotating Wind Turbine Blades in Stall*, Report ECN - C-93-052, 1994.

[32] Corrigan J.J. and Schillings J.J., *Empirical Model for Stall Delay Due to Rotation*, Aeromechanics Specialists Conference, San Francisco, CA (U.S.A.), January 1994.

[33] Costes J.J., Petot D. and Vansteenberghe J.F., *Etudes pour l'amélioration de la prévision du comportement d'un rotor d'hélicoptère*, Rapport Technique ONERA No. 10/4371 RY 030 R, 1994.

[34] Maier T.H. and Bousman W.G., *An Examination of the Aerodynamic Moment on Rotor Blade Tips Using Flight Test Data, and Analysis*, Eighteenth European Rotorcraft Forum,Avignon, France, paper No. 79, September 1992.

[35] Szafruga J. and Ramaprian B.R., *Pressure Measurements over the Tip Region of a Rectangular Wing - Part I. Stationary Wing*, AIAA 12th Aerodynamic Conference, Colorado Springs, CO (U.S.A.), June 1994.

[36] Beddoes T.S., *A 3-D Separation Model for Arbitrary Planforms*, AHS 47th Annual Forum, Phoenix, Arizona, May 1991.

[37] Leishman J.G. and Crouse G.L., *A State-Space Model of Unsteady Aerodynamics for Flutter Analysis in a Compressible Flow*, AIAA Paper 89-0022, 1989.

[38] Wake B.E. and Lorber P.F., *Dynamic Stall Correlation of a Rotor/Wing Navier-Stokes Solver on a Massively - Parallel Computer*, AHS 49th Annual Forum, St. Louis, MO (U.S.A.), May 1993.

[39]Costes J.J., *Aerodynamic Moments on Rotor Blades in Forward Flight: Test Results and Modelling*, Twenty First European Rotorcraft Forum, Saint-Petersburg, Russia, 1995.

[40] Berry J.D., *Measurement of Unsteady Flow Characteristics Behind a Model Helicopter Rotor*, AHS Northeast Region Aeromechanics Specialists Conference, Fairfield County, CT (U.S.A.), October 1995.

[41] Toulmay F., *Modèle d'Etudes de l'Aérodynamique du Rotor (METAR), Formulation et Application au SA 349 pales GV*, Rapport R371.76 Aérospatiale Div. Hélicoptère, 1986.

[42]Arnaud G. and Beaumier P., *Validation of R85/METAR on the Puma RAE Flight Tests*, Eighteenth European Rotorcraft Forum, paper No. 20, September 1992.

[43]Lyoen S., *Vitesse Induite Tourbillonnaire sur Rotor d'Hélicoptère*, Stage D.E.A. Mécanique, Université Lille I, Juillet 1995.

[44]Drevet J.P., *11ème campagne d'essais de rotors d'hélicoptères dans la soufflerie S1MA. Rotors 7A et 7AD1*, P.V. No. 5/8467GY, Tomes 1/2 et 2/2, Février 1992.

[45]Philippe J.J., *Survey of ONERA Code Development and Validation Studies for Multidisciplinary Research on Rotor Aeromechanics*, Aeromechanics Specialists Conference, San Francisco, CA (U.S.A.), January 1994.

[46]Tourjansky N. and Szechenyi E., *The Measurement of Blade Deflections*, Eighteenth European Rotorcraft Forum, Avignon, France, paper E10, September 1992.

[47]Hooper E.V., *The Vibratory Airloading of Helicopter Rotors*, Ninth European Rotorcraft Forum, Stresa, Italy, September 1983.

[48]Lim J.W. and Anastassiades T., *Correlation of 2GCHAS Analysis with Experimental Data*, Aeromechanics Specialists Conference, San Francisco, CA (U.S.A.), January 1994.

[49]Ormiston R.A., Rutkowski M.J., Ruzicka G.C., Saberi H. and Jung Y., *Comprehensive Aeromechanics Analysis of Complex Rotorcraft Using 2GCHAS*, Aeromechanics Specialists Conference, San Francisco, CA (U.S.A.), January 1994.

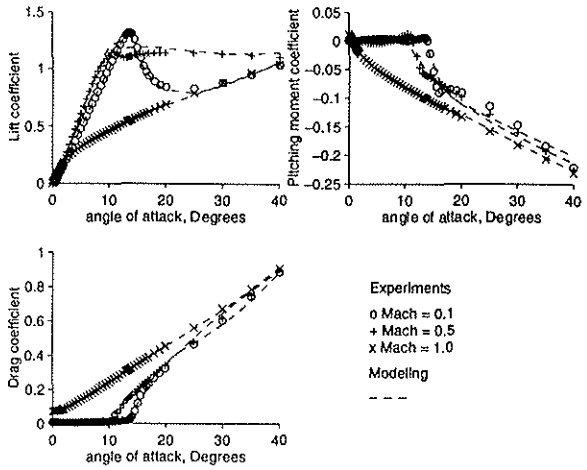

Fig. 1 - Modeling of the aerodynamic coefficients of the OA 209 airfoil.

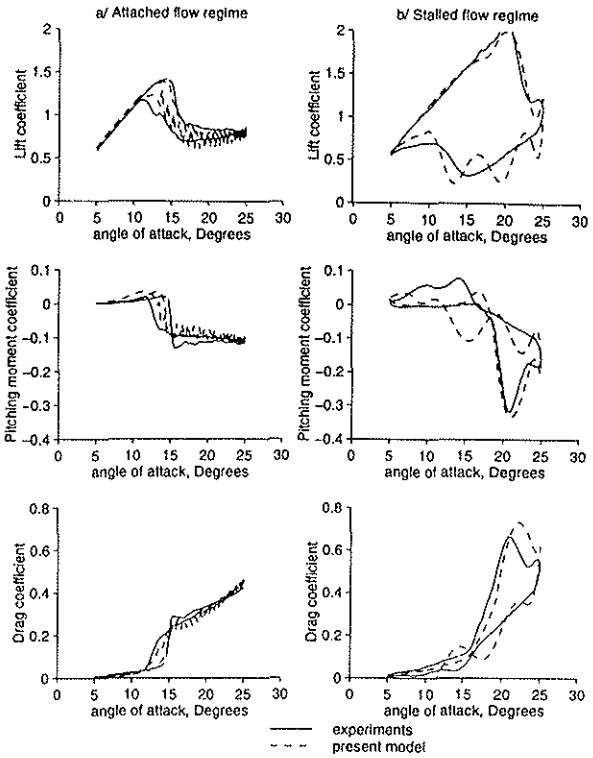

Fig. 2 - Comparison between experimental and calculated results of the aerodynamic coefficients for the NACA 0012 airfoil in deep stall.

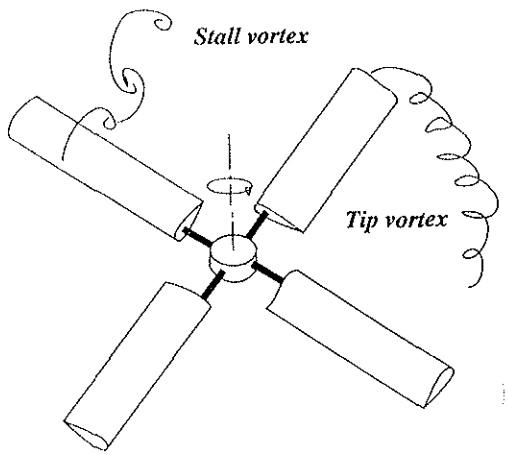

Fig. 3 - Flowfield around a rotor blade.

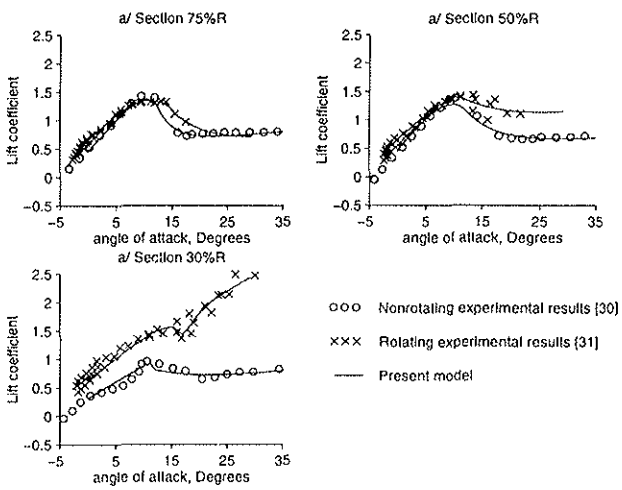

Fig. 4 - Rotation effects for a wind turbine.

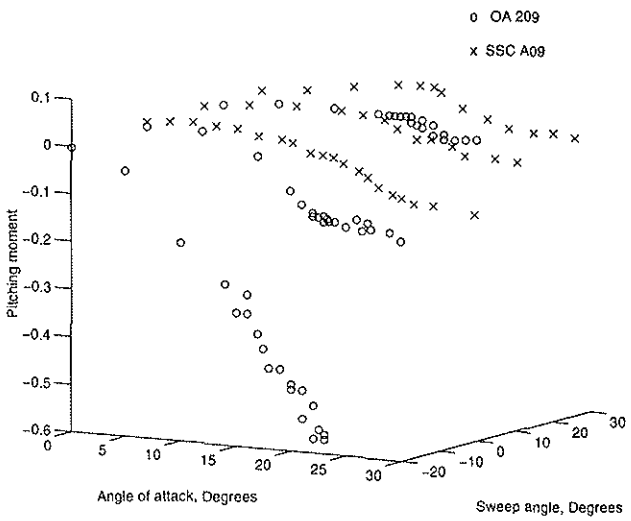

Fig. 5 - Measured values of pitching moment coefficient at the tip of two swept wings of different airfoil sections OA 209 and SSCA09.

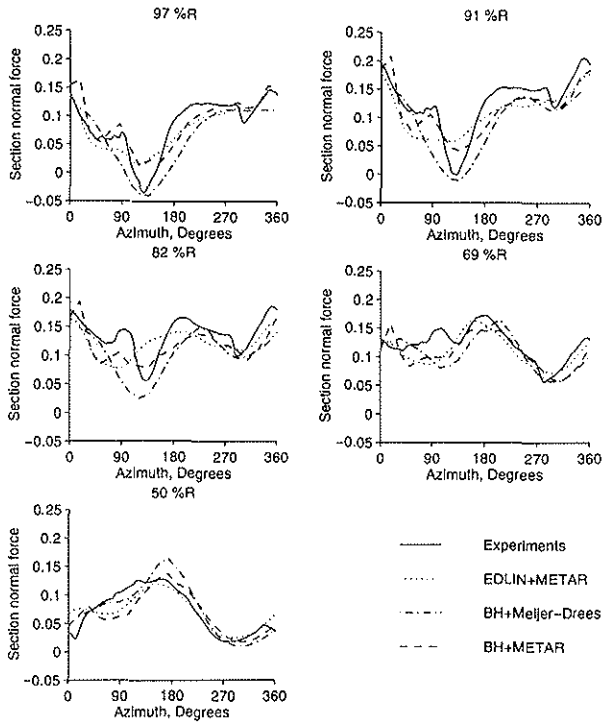

Fig. 6 - Measured and calculated sectional normal force $C_N M^2$ for test case with $C_L/\sigma = 0.08$ and $\mu = 0.30$ on the rotor with rectangular blades.

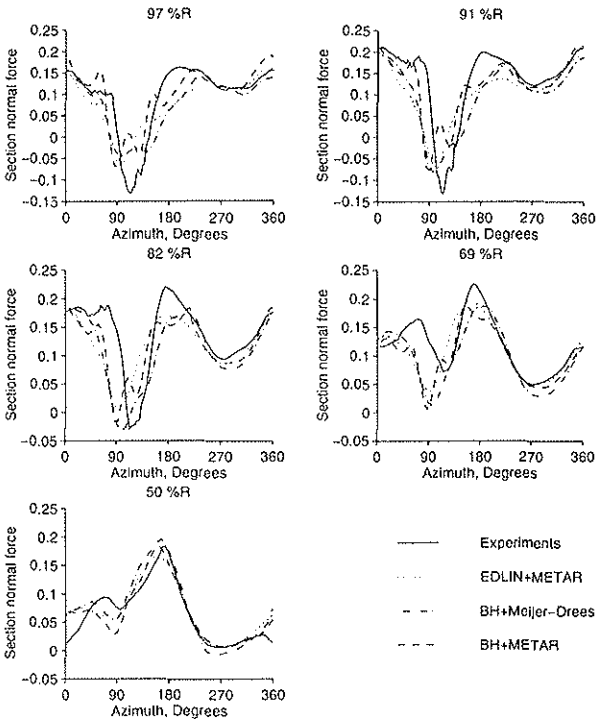

Fig. 7 - Measured and calculated sectional normal force $C_N M^2$ for test case with $C_L/\sigma = 0.08$ and $\mu = 0.40$ on the rotor with rectangular blades.

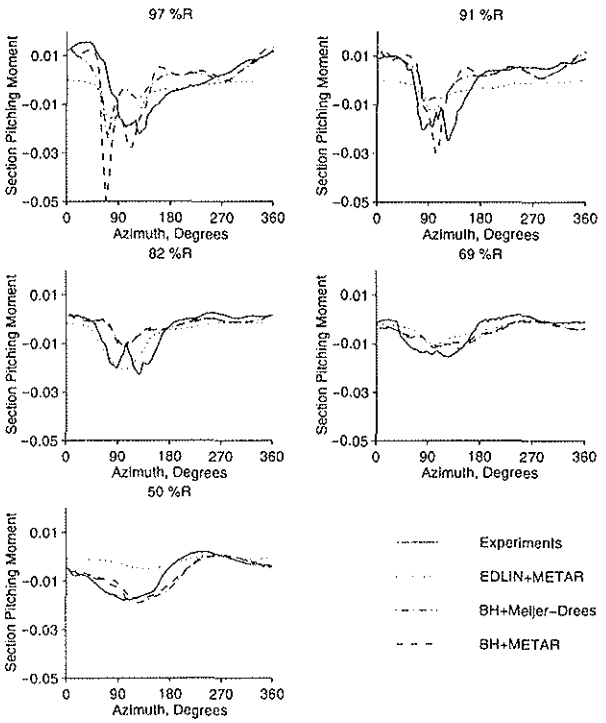

Fig. 8 - Measured and calculated sectional pitching moment coefficient $C_M M^2$ for test case with $C_L/\sigma = 0.08$ and $\mu = 0.40$ on the rotor with rectangular blades.

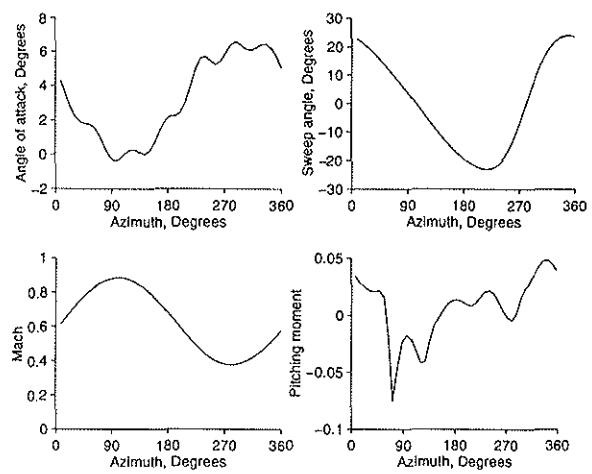

Fig. 9 - Calculated values of angle of attack, sweep angle, Mach number and pitching moment coefficient versus azimuth angle for test case with $C_L/\sigma = 0.08$ and $\mu = 0.40$ at the $97\%R$ blade section on the rotor with rectangular blades.

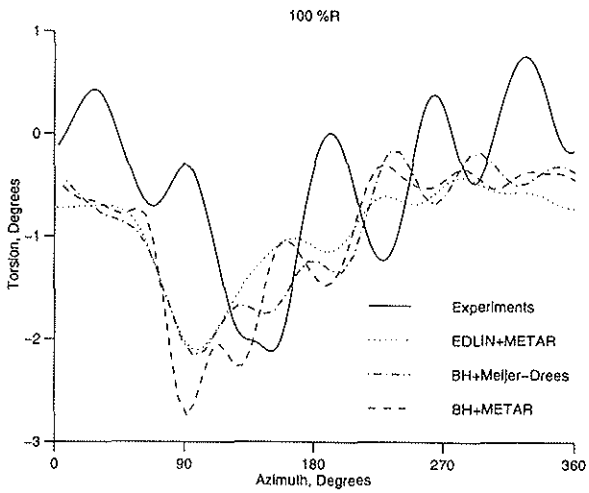

Fig. 10 - Measured and calculated blade tip deflection for test case with $C_L/\sigma = 0.08$ and $\mu = 0.40$ on the rotor with rectangular blades.

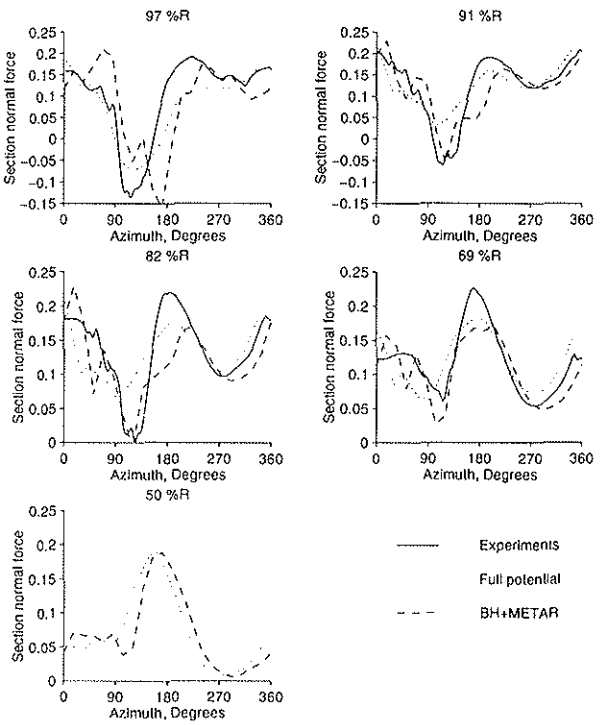

Fig. 11 - Measured and calculated sectional normal force $C_N M^2$ for test case with $C_L/\sigma = 0.08$ and $\mu = 0.40$ on the rotor with sweptback parabolic/anhedral blade tips.

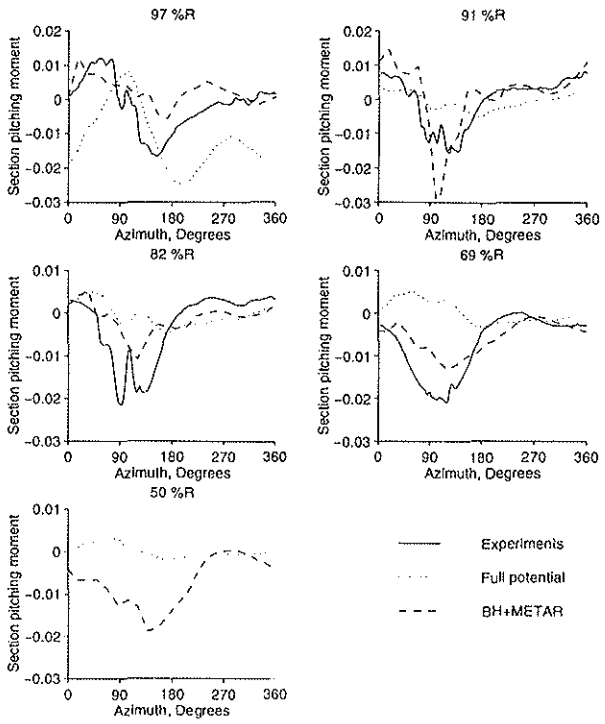

Fig. 12 - Measured and calculated blade sectional pitching moment coefficient $C_M M^2$ for test case with $C_L/\sigma = 0.08$ and $\mu = 0.40$ on the rotor with sweptback parabolic/anhedral blade tips.

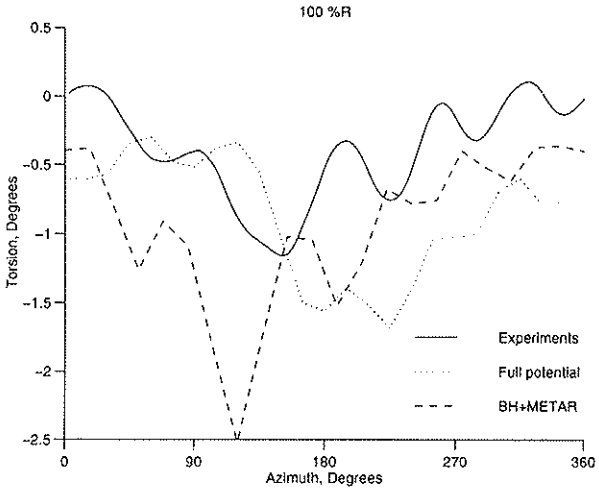

Fig. 13 - Measured and calculated blade tip torsional deflection for test case with $C_L/\sigma = 0.08$ and $\mu = 0.40$ on the rotor with sweptback parabolic/anhedral blade tips.

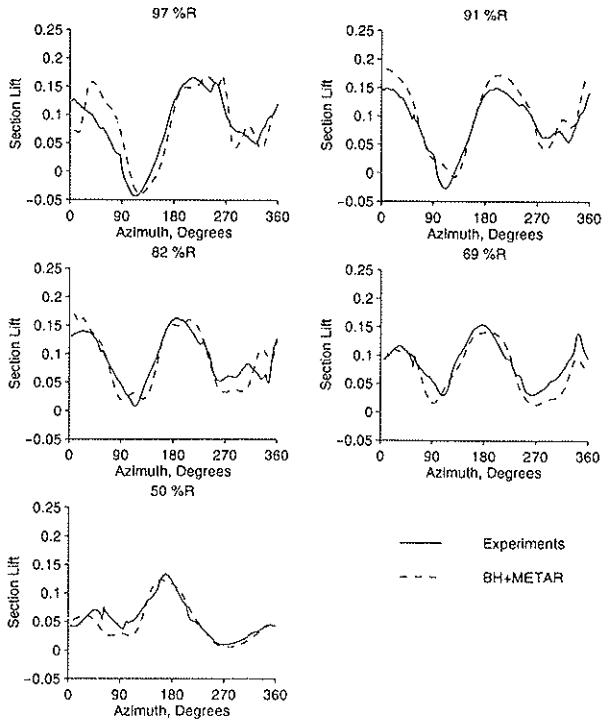

Fig. 14 - Measured and calculated section normal coefficient $C_N M^2$ fortest case with $C_L/\sigma = 0.11$ and $\mu = 0.40$ on the rotor with sweptback parabolic/anhedral blade tips.

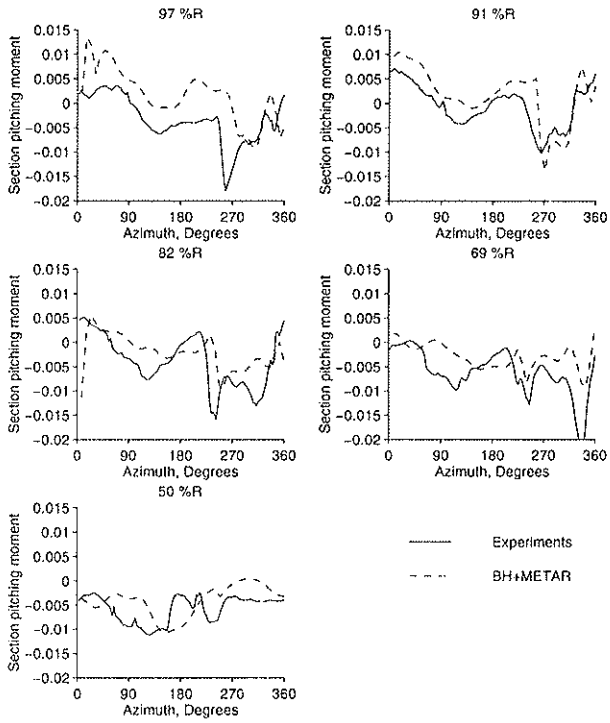

Fig. 15 - Measured and calculated blade sectional pitching moment coefficient for test case ($\mu = 0.40, C_L/\sigma = 0.10$) on the rotor with sweptback parabolic/anhedral blade tips.

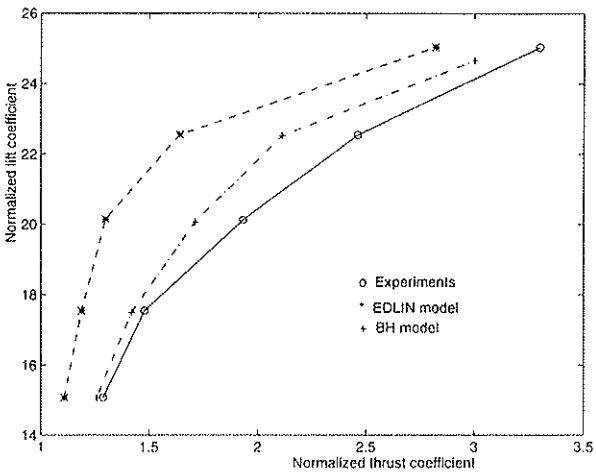

Fig. 16 - Rotor power for the rotor with sweptback parabolic/anhedral blade tips in stalled flow condition with advance ratio $\mu = 0.40$.